One-Pot Spray-Dried Graphene Sheets-Encapsulated Nano-Li4Ti5O12 Microspheres for a Hybrid BatCap System

1 AUTHOR:

Yu-Shi He

Shanghai Jiao Tong University

48 PUBLICATIONS   **791** CITATIONS

One-Pot Spray-Dried Graphene Sheets-Encapsulated Nano-Li$_4$Ti$_5$O$_{12}$ Microspheres for a Hybrid BatCap System

Tao Yuan,[†,‡] Wen-Ting Li,[†] Weimin Zhang,[†,‡] Yu-Shi He,[*,†] Chunming Zhang,[§] Xiao-Zhen Liao,[†] and Zi-Feng Ma[†,‡]

[†]Institute of Electrochemical and Energy Technology, Department of Chemical Engineering, Shanghai Jiao Tong University, Shanghai, 200240, China

[‡]Sinopoly Battery Research Center, Shanghai 200241, China

[§]National Engineering Research Center for Nanotechnology, Shanghai 200241, China

S Supporting Information

ABSTRACT: In this study, we report a facile strategy for constructing three-dimensional (3D) crumpled graphene sheets-wrapped nano-Li$_4$Ti$_5$O$_{12}$ (LTO@GS) composites using a one-pot spray-drying assisted solid-phase reaction method with anatase TiO$_2$ as a starting material. The proportion of graphene oxide (GO) in the LTO@GS composite greatly influences the phase formation and electrochemical performance of the composite. As an anode material for a nonaqueous, hybrid battery-capacitor (BatCap) system, the LTO@GS composite exhibits good high-rate capability and long cycle life. The specific capacitance still retains 90% of the initial value after 20 000 cycles, and the Coulombic efficiencies are close to 100%. This can reasonably be attributed to the interesting crumpled graphene-encapsulated structure and extraordinary synergistic effects between the two components.

1. INTRODUCTION

Due to the global energy crisis, climate abnormity, and environmental pollution, an extensive research effort has been paying to rechargeable batteries for applications in hybrid electric vehicles and stationary storage systems.[1,2] Li-ion batteries (LIBs) and electrochemical capacitors (ECs) are the most common types of energy storage systems.[3,4] However, in the current situation neither LIBs nor ECs can meet the requirements of practical applications. For example, LIBs exhibit a high energy density of 120−200 Wh kg^{-1}, while exhibiting a relatively low power density and short cycle-life. Although EC displays the opposite performance with a high power density of 2−5 kW kg^{-1} and outstanding cycle performance, its specific energy is very low at only 2−5 Wh kg^{-1}.[5,6] In order to make best of the merits of both LIB and EC, it was suggested to combine the two energy devices into one system which may deliver high energy and power densities simultaneously. Amatucci's group first combined the LIBs anode material of LTO with an active carbon (AC) cathode electrode, designing a new device called a "BatCap" hybrid system with 2.8 V potential ranges and more than 10 Wh kg^{-1} of specific energy.[7] Following this pioneering work, many researchers have devoted intensive efforts to the BatCap system.[8−16]

In the BatCap system, Li intercalation into the anode plays a very important role which requires highly rated performance, long-term stability, and safety. So far, several lithium-insertion type materials such as LTO,[8,9] TiO$_2$,[10,11] NiCo$_2$O$_4$,[12] LiTi$_2$(PO4)$_3$,[13] TiP$_2$O$_7$,[14] LiCrTiO$_4$,[15] and graphite[16] have been proposed as alternative host materials. Among the materials, spinel-type LTO has been receiving particular interest because of its unique properties with an appropriate

discharge voltage (1.55 V vs Li/Li$^+$), ensuring a high operational safety by avoiding the formation of dendritic lithium and a solid electrolyte interphase. In addition, negligible volume variation during the electrochemical reactions leads to high cycling stability. And the very flat charge/discharge platform can be employed as an easy indication of the end of charge or discharge.[17]

However, common LTO has low electronic conductivity (ca. 10^{-13} S·cm^{-1})[18] and a moderate Li$^+$ diffusion coefficient (<10^{-13} cm^2 s^{-1});[19] thus poor power capability is frequently obtained for coarse LTO.[20] In order to improve the power capability of LTO, decreasing the particle size, doping, and the surface coating methodology are the most commonly used strategies.[21−23] Among the modified schemes, combining LTO with GS by use of a specific property of graphene, such as the special one-dimensional morphology, excellent electrical conductivity, and abundant surface functional groups, has been proven to demonstrate superior rate capability for LIBs and supercapacitors in previous works.[9,24−27] Many efforts have been made to prepare high-performance LTO@GS composites, such as using sol−gel,[24] hydrothermal,[25] and solvothermal[26] methods. It is noticeable that, in most of the above cases, expensive organic solvents containing Ti as raw materials were required, which, however, increases the cost. In addition, multisteps synthesis strategies are the most common method and have proved complicated, which typically includes synthesis of LTO and then combination with GO or GS.[9,27] For practical

application, the ideal synthetic technique should meet the requirements of a facile process, low cost, and easy scale-up.

The spray-drying technique, due to the simple apparatus and easy scale- up, has been widely used for synthesis of functional nanoparticles or special core—shell structure encapsulation for mass production in the field of chemical engineering and materials.[28−30] This technique is also inferential to be suitable for preparing 3D GS. For example, Luo et al. reported crumpled graphene balls via the capillary force resulting from rapid solvent evaporation and physical shrinkage of aqueous two-dimensional GO sheets during an aerosolization process.[31] The crumpled 3D GS not only increases the specific surface area and reactive sites of the products for the electrochemical reaction but also exhibits excellent stability when it undergoes redispersion, heating, or other material processing treatments.[32−34] When compounding with other functional materials, the GS can encapsulate functional materials simultaneously during the shrinkage process, which will form graphene-wrapped materials with special properties.[35−38]

Previously, our group successfully applied this method to prepare Si@GS and Fe_2O_3@GS composites for LIB application.[35,38] In this work, we developed GS encapsulated nano-LTO microspherical composites with a 3D structure as anode materials for the BatCap system using a one-pot spray-drying assisted solid-phase reaction method with anatase TiO_2 as a starting material. The key strategy in this work is to fully harness synergetic effects between LTO and GS. A 3D continuous and highly conductive network provided by GS can dramatically improve electronic conductivity and shortened ion transport paths of LTO. Moreover, GS can effectively mediate the crystalline growth of the spinel LTO phase to obtain nanostructure LTO which is beneficial to rapid Li^+ diffusion. On the other hand, the dispersed LTO nanoparticles can suppress the agglomeration and restacking of GS. In addition, using inexpensive and environmentally friendly titanium oxide instead of expensive organic materials as the reactant has a great advantage in economy and large-scale industrial implementation. The electrochemical evaluations have been systematically carried out in this study, and the LTO@GS hybrid is proved to be an ideal anode material for the hybrid BatCap system, which exhibits highly rated performance and excellent cycle stability.

2. EXPERIMENTAL SECTION

Synthesis of LTO@GS Microspheres. Graphite oxide was synthesized from natural graphite powder (Grade 230, Asbury Carbons) using a modified Hummer's method.[39] The equipment and typical procedure for the synthesis of LTO@GS is shown schematically in Figure 1. The graphite oxide was exfoliated into deionized water by sonication to form a graphene oxide (GO) suspension. Anatase-type TiO_2 solid (particle size: ~10 nm; specific surface area: 54.4 m^2 g^{-1}) was used as a titanium source and $LiNO_3$ as a lithium source. Note that the Li source was 3% mole excessive to the Ti source, ensuring that the Li was sufficient for the reaction. Thereafter, a certain amount of active material was added into the GO suspension (1 mg mL^{-1}) with a mass ratio of LTO to GO of 80:20. The mixture was sonicated for 1 h. The well-dispersed aqueous mixtures were supplied into a B-290 mini spray drier (Buchi, Swiss) continuously by a peristaltic pump and then nebulized to aerosol droplets through a nozzle carried by a preheated air stream and subsequently flowed through the cylinder. The inlet air temperature in the spray-drying process
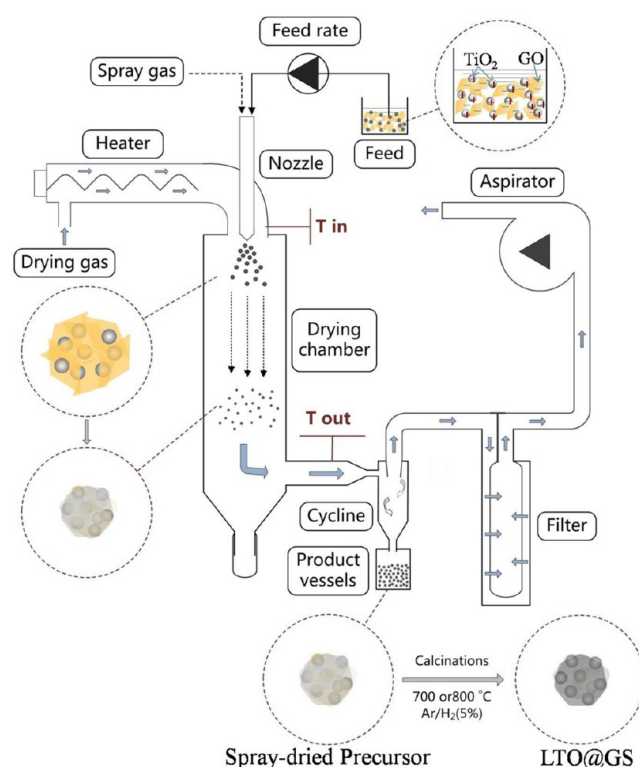

Figure 1. Schematic of the synthesis route of LTO@GS composites.

was maintained at 200 °C. In the cylinder, the aqueous solvents were evaporated rapidly, and GO sheets shrank as a result of capillary stress and encapsulated all the reaction materials including Li^+ and nano-TiO_2 particles under the effects of evaporation.[35,38] The solid products of GO-wrapped Li^+−TiO_2 hybrid microspheres were collected in the product vessels driven by the cyclone, which were designated as spray-dried precursor A (SP-A). SP-B, SP-C, and SP-D were synthesized by the same method, except that the weight ratios of LTO to GO were 75:25, 70:30, and 65:35, respectively. The obtained GO−Li^+−TiO_2 hybrid microspheres were calcined in a stream of argon/hydrogen (5%) at 700 and 800 °C for 3 h, respectively, to convert into spinel type LTO@GS composites.

Structural and Morphological Characterization. X-ray diffraction (XRD) measurements were carried out using a Rigaku D/MAX-2200/PC X-ray diffractometer at 40 kV and 20 mA, with a Cu Kα radiation source. An X-ray photoelectron spectrometer (XPS, Kratos Axis Ultra DLD) was utilized to analyze the surface properties of the samples. Thermogravimetric analysis (TGA) was performed using a STA 449F3 analyzer (NETZSCH Co., Germany) to determine the residual level of LTO@GS composites after calcination. The morphology and microstructure of the samples were monitored using a FEI Nova SEM 230 ultrahigh resolution Field Emission Scanning Electron Microscope (FE-SEM; INCA X-Max 80, Oxford Instruments) and Transmission Election Microscopy (TEM) and High-Resolution Transmission Election Microscopy (HR-TEM; JEM-2100F, JEOL Ltd., Japan). Porosity and Brunauer−Emmett−Teller (BET) surface areas for the samples were measured using a nitrogen sorption instrument (Micromeritics, ASAP2020).

Electrochemical Measurements. Electrochemical analyses were carried out using 2016 coin cells for the LTO@GS||Li system and monolithic soft packed cells (50 mm × 50

mm) for the BatCap (LTO@GS‖AC) system at room temperature (about 25 °C).

For the LTO@GS‖Li system, the LTO@GS electrodes were prepared using a slurry containing 85 wt % active material, 8 wt % carbon black, and 7 wt % polyvinylidene fluoride (PVDF). The electrodes were dried in a vacuum oven at 100 °C for 24 h before being transferred to the glovebox. The coin cells were assembled with lithium−metal as the counter and reference electrode, Celgard 2400 as the separator, and 1 M $LiPF_6$/EC/DMC (1:1 by volume ratio) as the electrolyte in the glovebox. The electrochemical performances were tested at various charge/discharge rates in the potential range 1.0–3.0 V vs Li/Li^+ using a LAND CT2001A model battery test system (Wuhan Jinnuo Electronics, Ltd.) under constant current conditions.

For the BatCap (LTO@GS‖AC) system, the LTO@GS anodes were also prepared as above-mentioned. The thickness of the anodic electrode was 20 mm with a loading of active material weight of about 2.6 mg cm^{-2}. Activated carbon (AC; Kuraray YP-50F, Japan, surface area of 1700 $m^2 g^{-1}$) electrodes were prepared using 85 wt % active material, 5 wt % carbon black, and 10 wt % LA133 (water-based binder). The mass ratio of cathodic active material to the anodic material was close to 4:1. This ratio was calculated based on the theoretic-specific capacity of LTO and AC.[40] Soft packed cells (LTO@GS‖AC) were assembled with NKK TF40 as the separator and 1 M $LiPF_6$/EC/DMC/EMC (1:1:1 by volume ratio) as the electrolyte in a glovebox. The BatCaps were charged/discharged at 1.5−3 V at various current densities from 20 to 1600 mA g^{-1} in constant-current mode. The specific capacity and electrochemical rate always refer to the total weight of the active materials in the anodes and cathodes. For reference, an AC‖AC electric double layer capacitor was also assembled using the same method mentioned above.

The AC electrochemical impedance spectroscopy (EIS) tests of the cells were carried out on a Solartron FRA 1260 frequency response analyzer combined with a Solartron SI 1287 Electrochemical Interface with an amplitude of 10 mV at a frequency range from 100 kHz to 0.01 Hz.

3. RESULTS AND DISCUSSION

Anatase-TiO_2, $LiNO_3$, and GO with various mass ratios were ultrasonically mixed using deionized water as a solvent to form a well-dispersed aqueous colloid suspensions. There were no stratification and precipitation phenomena after 12 h, indicating that TiO_2, $LiNO_3$, and GO uniformly dispersed in the solvent. Normally, the functional groups on the GO surface are negatively charged,[41] while the nano-TiO_2 surface shows positive charge.[42] Therefore, GO, TiO_2, and Li^+ could attract each other for the static effect, which leads to a good precondition for subsequent spray-drying process. The FE-SEM images of SP-A, -B, -C, and -D obtained by the spray-drying process are shown in Figure S1, which exhibits spherical secondary particles with a diameter of ∼2 μm (insets in Figure S1) and consists of numerous GO-wrapped TiO_2 nanoparticles. With an increase in the contents of GO, the degree of encapsulation becomes more evident. The XRD patterns of spray-dried precursors are shown in Figure 2a. The major diffraction peaks at 2θ matched with the characteristics of anatase-type TiO_2 (JCPDS 71-1166). Furthermore, the broad diffraction peak observed in SP-B, -C, and -D between about 24° and 28° is attributed to GS.[35,38] There are no clear characteristics of GO at about 11° in all samples,[43] which
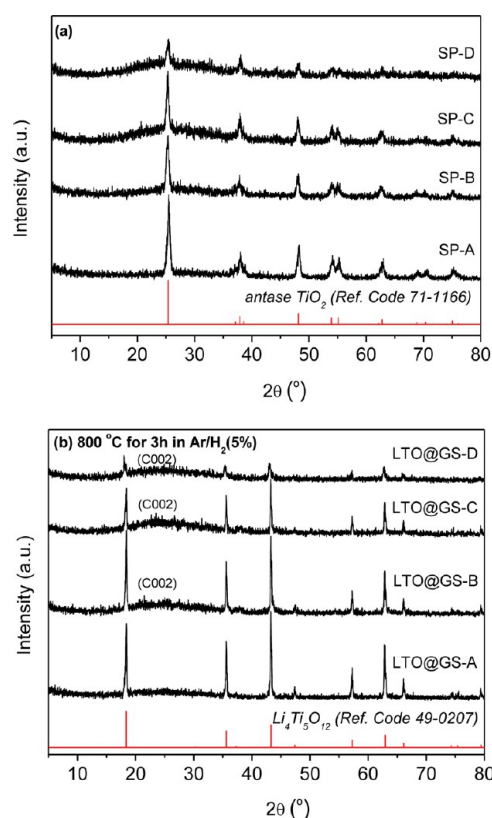

Figure 2. XRD patterns of (a) spray-dried precursors and (b) LTO@GS composites calcined at 800 °C for 3 h in Ar/H_2 (5%).

indicates that GO has been partially reduced to GS during the preliminary spray-drying process.[38]

In order to completely reduce the GO and form the spinel LTO phase, the spray-dried precursors were calcined at 700 and 800 °C in Ar/H_2 (5%) for 3 h, respectively. The products obtained from SP-A show gray-blue color, while those from SP-B, -C, and -D are black. The gray-blue color is due to the Ti^{4+} in the surface partly reduced into Ti^{3+} for both the effects of GO and reduced calcination atmosphere.[21,44] Similarly, Ti^{3+} should also present in the other three samples. The reports elsewhere demonstrated that the presence of Ti^{3+} was beneficial to enhancing the kinetics of Li diffusion by at least 1 order of magnitude.[21,45] Therefore, the enhanced electrochemical reaction kinetics of LTO@GS samples may be expected to occur in the device that is operating.

From the XRD results shown in Figure S2, after 700 °C calcination in Ar/H_2 (5%) for 3 h, a high-purity and well-crystallized LTO phase (JCPDS 49−0207) is obtained from SP-A. However, a considerable amount of TiO_2 anatase is observed in the calcined SP-B, -C, and -D products. When the calcination temperature rises to 800 °C, pure phased spinel LTO is formed in all products (Figure 2b), which are designed as LTO@GS-A, -B, -C, and -D, correspondingly. Furthermore, broad diffraction peaks (C002) of GS shown between 24° and 28° are quite visible in the XRD patterns of LTO@GS-B, -C, and -D samples. However, this diffraction peak is not clear in LTO@GS-A. It is also noteworthy that the intensities of spinel LTO diffraction peaks are decreased accordingly with an increase of the contents of GO; this may be partly caused by the GS covering, which weakens the XRD signal intensity of LTO. Another reason may be ascribed to the smaller particle size of the products. The crystallite sizes of LTO@GS-A, -B, -C,
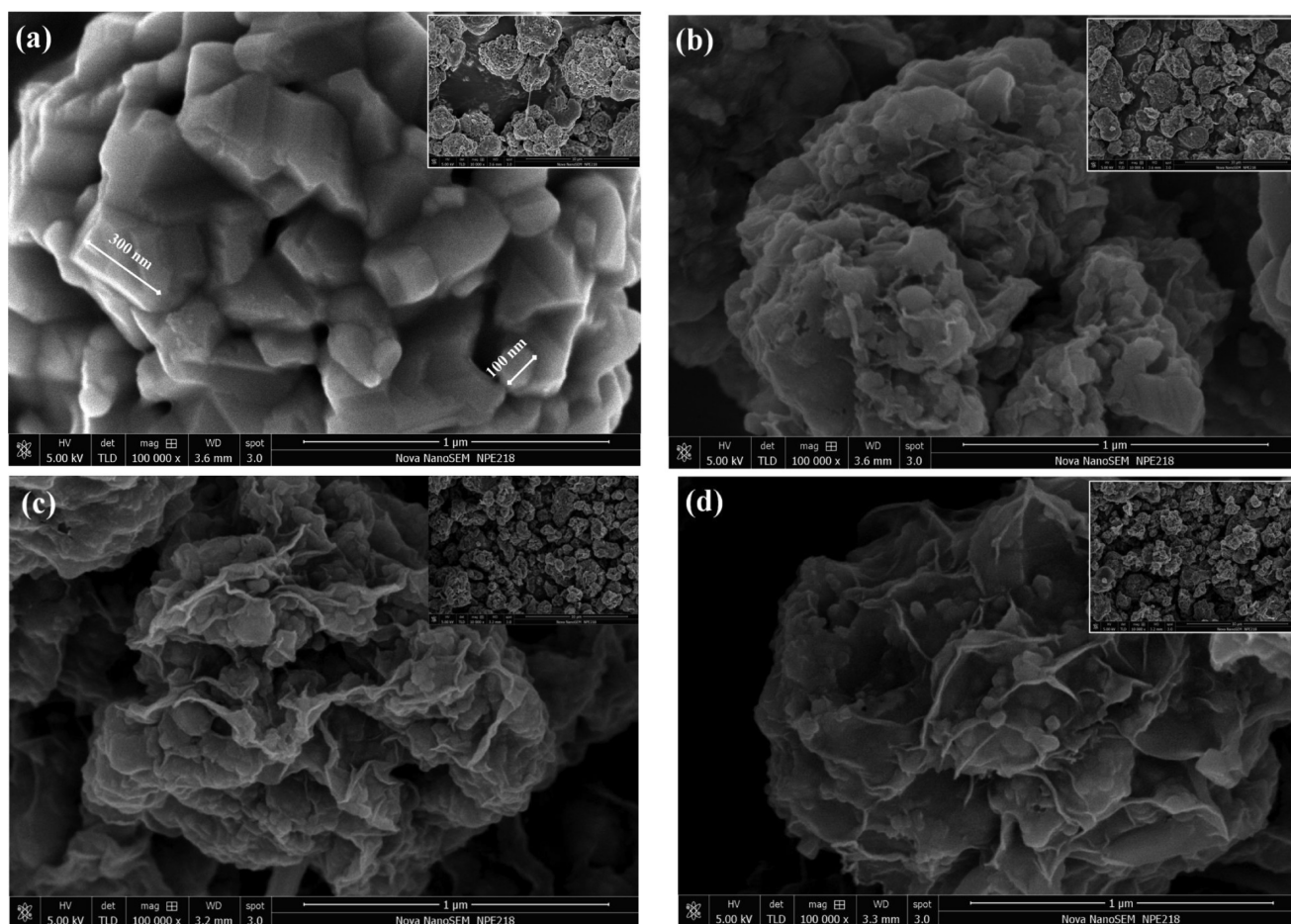
Figure 3. FE-SEM images of (a) LTO@GS-A, (b) LTO@GS-B, (c) LTO@GS-C, and (d) LTO@GS-D (insets: overall images).

and -D calculated based on the XRD using the Scherrer equation are 56.8, 44.2, 38.9, and 20.9 nm, respectively. However, due to the relatively low content of Ti^{3+} in the LTO@GS sample, the related Ti^{3+} phase cannot be identified by XRD. We carried out XPS investigation to further confirm the chemical state of Ti ions in the LTO@GS composites. Shown in Figure S3 are the high-resolution XPS spectra of the Ti 2p of LTO@GS composites. The results indicate the presence of Ti^{3+} species in all of the LTO@GS samples.

To determine the amount of graphene in the LTO@GS composites, TGA was carried out at a heating rate of 10 °C min^{-1} from 40 to 800 °C in the air. Based on the TGA results (Figure S4), the contents of GS in the pure spinel phased LTO@GS-A, -B, -C, and -D samples are 0%, 1.93%, 4.46%, and 6.63%, respectively. Because $LiNO_3$ was used as a Li source, a small amount of oxygen would be released from precursors during the calcination process. So the GS in LTO@GS-A are completely consumed due to the low initial GO content in SP-A. And the contents of GS in the other samples increase according to the content of GO in the precursors. The Raman spectra of LTO@GS-B, -C, and -D show carbon D and G bands at 1355 and 1600 cm^{-1}, respectively (Figure S5). The intensity ratio of the D band and G band (I_D/I_G) offers useful information to evaluate the degree of crystallinity of GS.[46] In the present Raman spectra, the intensity ratios of LTO@GS-B, -C, and -D composites are calculated to be 1.7, 1.8, and 1.5, respectively, which indicates that the obtained GS in LTO@

GS-B, -C, and -D samples are predominantly hybridized in an sp^2 manner, thereby possessing good electronic conductivity.[13]

We carried out FE-SEM to investigate the morphologies of pure phased spinel LTO@GS composites. As shown in Figure 3a, LTO@GS-A is sintered seriously, and the particle size grows greatly to about 100−300 nm, which may be caused by the lack of barrier effect of the GS. While the other three samples in Figure 3b−d are present, there is the typical crinkled and rippled morphology of GS, and the particle structure becomes more open than the spray-dried precursors, which is similar to peonies. The particle sizes of LTO are 20−40 nm in LTO@GS-B, -C, and -D samples. The BET surface areas of LTO@GS-A, -B, -C, and -D from the N_2 absorption measurement are 3.5, 15.7, 20.3, and 22.8 $m^2 g^{-1}$, respectively. According to the FE-SEM results, the increased specific surface areas may be assigned to the nanostructure of nanosized LTO particles and GS. Moreover, the Barrett−Joyner−Halenda (BJH) and nitrogen adsorption−desorption curves in Figure S6 demonstrate that LTO@GS-B, -C, and -D samples exhibit a porous structure with a mean pore size of 2−4 nm, which is expected to provide very regular pore channels for charge transfer.

The morphologies of the GS coated samples were further investigated using TEM and HR-TEM. Figure 4a, b, and c (left) reveal that the GS uniformly distributes on/in the micrometer-sized LTO@GS spheres and further establishes a conductive network through the whole microsphere. The particle size of LTO is 20−40 nm, which is consistent with the FE-SEM images. Furthermore, as revealed by the HR-TEM images in
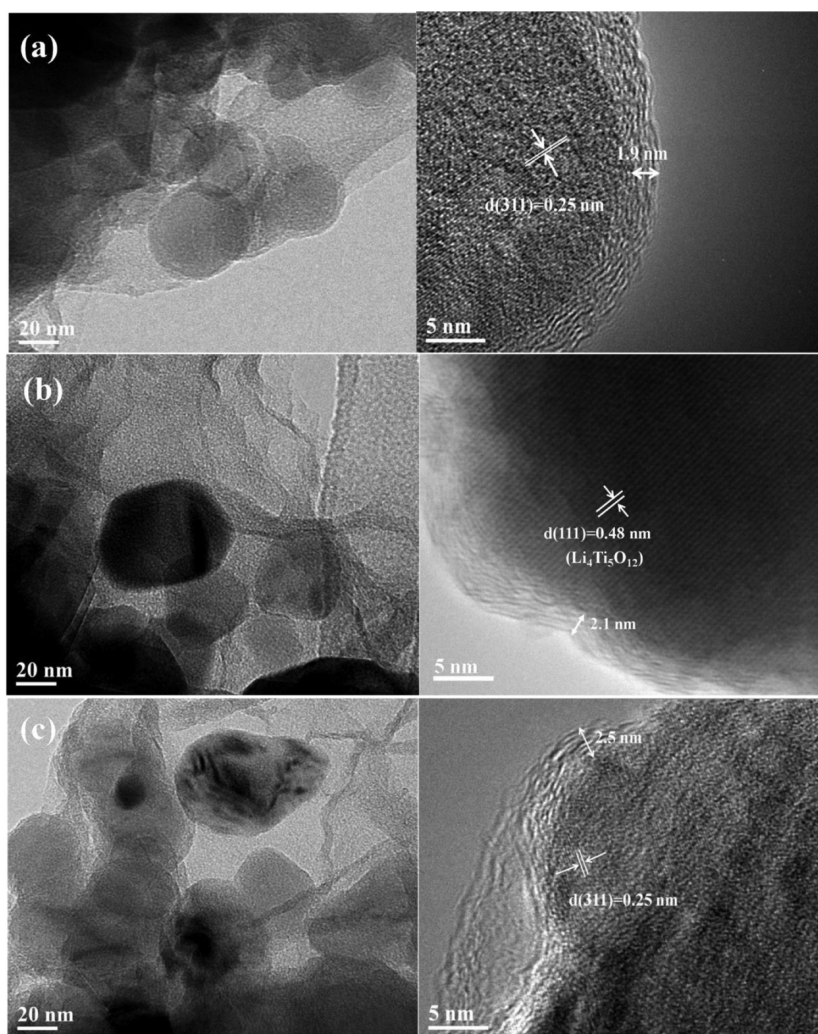
10852

dx.doi.org/10.1021/ie501287a | Ind. Eng. Chem. Res. 2014, 53, 10849−10857

Figure 4. TEM images of a local area on LTO@GS composites (left) and HR-TEM images on the edge of LTO particles (right) of (a) LTO@GS-B, (b) LTO@GS-C, and (c) LTO@GS-D samples.

Figure 4a, b, and c (right), crystallized LTO can be clearly observed in LTO@GS-B, C, and D samples, which were indexed to the crystal faces (3 1 1), (1 1 1), and (3 1 1), respectively. The coated GS layer has a thickness of about 1.9, 2.1, and 2.5 nm of LTO@GS-B, -C, and -D, respectively.

From the above discussion, we can conclude that the GO contents in the spray-dried precursors significantly influence the structure and morphology of the final products. In our previous study, we observed that the carbon layer around the TiO_2 particles would hinder the transfer of Li^+ to some extent.[47] Since LTO@GS-A does not have a barrier effect of the GS, pure phased spinel LTO can be formed at a lower calcination temperature of 700 °C. While the pure phased spinel LTO@GS samples with more GO in the precursors must be obtained at a higher calcination temperature up to 800 °C. However, the presence of the GS layer effectively restricts the growth of LTO primary particles during solid-state sintering and thereby controls their size on the nanometer scale. Meanwhile, the even GS coating net could be expected to reduce electric resistance of the electrode. Therefore, with ensuring a sufficient conductive network of GS to encapsulate all LTO particles, small amounts of GO in the precursor are desirable, which may facilitate Li^+ diffusion in the LTO@GS composites.

Electrochemical Performances of the LTO@GS Composites. As shown in Figure 5, the rate capacities of the LTO@GS materials were examined by using a LTO@GS‖Li half cell at various rates from 1 C to 40 C in the potential range of 1.0−3.0 V vs Li/Li$^+$. The corresponding rate charge/discharge curves are shown in Figure S7. At a charge/discharge rate of 1 C (170 mA g^{-1}), LTO@GS-B and LTO@GS-C
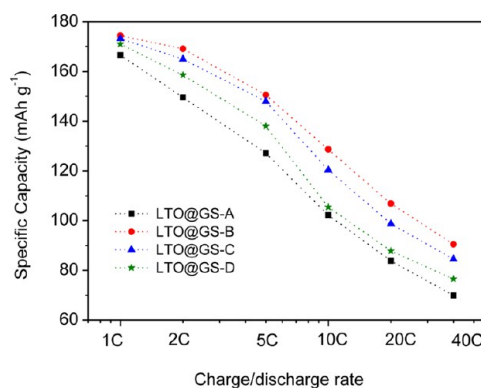

Figure 5. Rate capacities of LTO@GS composites as half-cell in a potential range of 1.0−3.0 V vs Li/Li$^+$.

exhibit specific capacities of 174.4 and 173.2 mAh g^{-1}, respectively, which is close to the theoretical value of 175 mAh g^{-1}. At the same current density of 1 C, the LTO@GS-A and LTO@GS-D show comparable capacities of 166.6 and 171.0 mAh g^{-1}, respectively. For LTO@GS-A, LTO grains inside the agglomerated particles are electro-active due to sufficient diffusion time; for LTO@GS-D, a hinder effect of thick stacked GS on diffusion of Li$^+$ at a 1 C rate is negligible. However, with an increase of the charge/discharge current rate, the difference between the lithium storage capacities of LTO@GS composites becomes evident. LTO@GS-B and LTO@GS-C are found to exhibit good capacity retention performance. At a discharge rate of 10 C, reversible capacities of 128.7 and 120.4 mAh g^{-1} are obtained, respectively. In comparison, LTO@GS-B shows the highest charge/discharge capacity in all samples regardless of the rate, which maintains 51.9% capacity (vs 1 C) even at a high charge/discharge rate of 40 C. However, the capacities of LTO@GS-A and LTO@GS-D drop more rapidly, retaining only 102.2 and 105.4 mAh g^{-1} at 10 C and 69.9 and 76.5 mAh g^{-1} at 40 C, respectively. This may be due to the lack of GS conductive matrix and a large portion of LTO@GS-A grains and a stacked GS coating layer of LTO@GS-D. The polarization process can also be clearly seen from Figure S7, with the values of the plateau potentials margin for LTO@GS-B and LTO@GS-C much smaller than those of LTO@GS-A and LTO@GS-D at all discharge rates from 1 C to 40 C.

To further understand the different electrochemical performance at high charge/discharge rates of LTO@GS samples, we record EIS measurement for all electrodes. The EIS result (Figure S8) shows that each curve consists of a depressed semicircle at the high-to-middle frequency region and an oblique straight line in the low frequency region. As the fitted results summarized in Table S1, LTO@GS-B, -C, and -D exhibit much lower ohmic resistance (R_s), charge transfer resistance (R_{ct}), and polarization resistance (R_f) than those of LTO@GS-A. Furthermore, the chemical diffusion coefficient of Li$^+$ inside LTO@GS samples (Figure S9 and Table S1) demonstrates that the Li$^+$ ion diffusion kinetics of LTO@GS-B and LTO@GS-C are significantly improved over those of LTO@GS-A and LTO@GS-D.

A full BatCap system cell test with LTO@GS-B as the anodic electrode and AC as the cathodic electrode was performed, which was designated as LTO@GS∥AC for simplicity. The setup is shown in the inset of Figure S10. Figure 6a shows the charge/discharge profile of LTO@GS∥AC BatCap with a current density of 20 mA g^{-1} and 40 mA g^{-1} (refer to the total weight of the active materials in the anodic and cathodic electrodes) corresponding to a 1C and 2 C rate in the range of 1.5–3.0 V. An AC∥AC symmetrical electric double layer capacitor (EDLC) was tested using the same cell and the same current density for comparison, as shown in Figure 6b. A linear charge/discharge profile of AC∥AC EDLC represented a typical double layer formation, which is in agreement with previous reports on nonaqueous EDLC systems.[40,48] Compared with AC∥AC EDLC, the charge/discharge curve of the LTO@GS∥AC BatCap system is not strictly linear, corresponding to the Li$^+$ lithiation/delithiation reaction in the LTO@GS anodic electrode. That indicates that the hybrid BatCap exhibited discharge characteristics of the combination of a battery and a capacitor. It is should also be noticed that the charging and discharging time of LTO@GS∥AC BatCap was significantly increased, corresponding to a higher energy density.
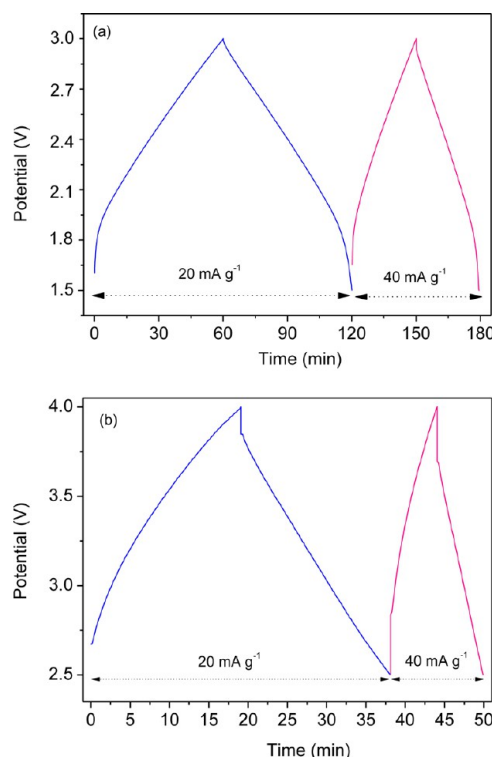

Figure 6. Charge–discharge curves of the (a) LTO@GS∥AC hybrid BatCap and (b) AC∥AC symmetrical EDLC at current density of 20 mA g^{-1} and 40 mA g^{-1}, respectively.

The rate capability of LTO@GS∥AC BatCap was examined at various discharge rates from 1 C (20 mA g^{-1}) to 80 C (1600 mA g^{-1}) as shown in Figure S10. As the current rate increases, the discharge time is reduced accordingly. At a high charge/discharge rate of 80 C, the discharge time remains 28 s. The discharge specific capacity C_m is from 37 to 48 F g^{-1} at various charge/discharge rates, which is calculated using formula 1:

$$C_m = \frac{i \times \Delta t}{m \times \Delta V} \tag{1}$$

(where i (in amperes) is the discharge current, ΔV (in volts) is the discharge voltage change (exclude the iR drop), and Δt (in seconds) is the discharge time consumed in the voltage change range of ΔV.)

The Ragone plots in Figure 7 summarize the specific energy and power densities of the LTO@GS∥AC BatCap system and conventional AC∥AC EDLC system, respectively. The result in Figure 7a demonstrates that the specific energy is 29.2 Wh kg^{-1} at a power density of 58.4 W kg^{-1}; when the power output reaches 1782.7 W kg^{-1}, the specific energy retains 13.4 Wh kg^{-1}. The energy density is 3 times that of a conventional AC∥AC symmetrical EDLC system,[48,49] and comparable with the results of other LTO∥AC hybrid BatCaps.[48,50,51] The corresponding remarkable increase in volumetric energy density in comparison with the commercial AC∥AC symmetrical EDLC system can be seen in Figure 7b. The performance enhancement can be ascribed to the synergistic effects between LTO and GS.

The cycle life result of the LTO@GS∥AC BatCap at a rate of 80 C is shown in Figure 8. The hybrid BatCap displays a sustained stability over a long cycle time at such a high cycle rate. After 20 000 cycles, the specific capacitance retains 90% of the initial value, and the Coulombic efficiencies are close to
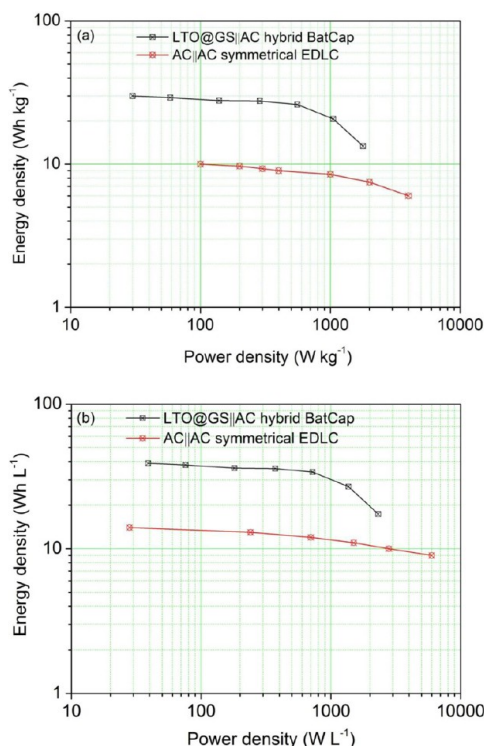
Figure 7. Ragone plots of (a) gravimetric and (b) volumetric energy and power densities of the LTO@GS‖AC hybrid BatCap and conventional AC‖AC symmetrical EDLC system.
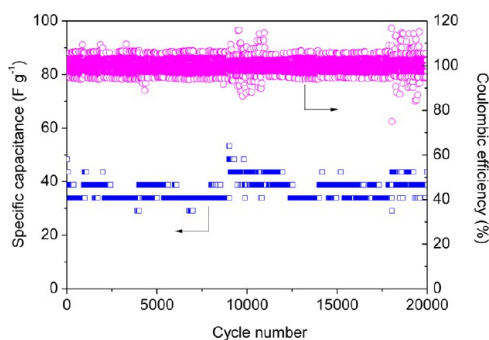

Figure 8. Specific capacitance based on both specific capacitance and Coulombic efficiency vs cycle number of the LTO@GS‖AC hybrid BatCap at 80 C rate (1600 mA g^{-1}).

100%. To understand the excellent cycling property of the LTO@GS‖AC hybrid BatCap, EIS experiments were carried out before cycling and after 20 000 cycles on the open circuit voltage of 1.9 V. As shown in Figure 9, the semicircles in the high frequency region of the two impedance curves coincide very well, which indicated that the ohmic resistance change of LTO@GS‖AC BatCap is negligible even after 20 000 cycle times. This explains the stable capacity of the LTO@GS‖AC BatCap upon cycling.

In summary, spherical GS-encapsulated LTO nanoparticle composites are constructed by a one-pot spray-drying assisted solid-phase reaction process. The GS layer can effectively restrict the LTO particle size growth and establish a continuous conductive network through the microspheres. On the other hand, the dispersed LTO nanoparticles can suppress the agglomeration and restacking of GS. The optimized electrochemical performance is obtained with a GS content of 1.93%
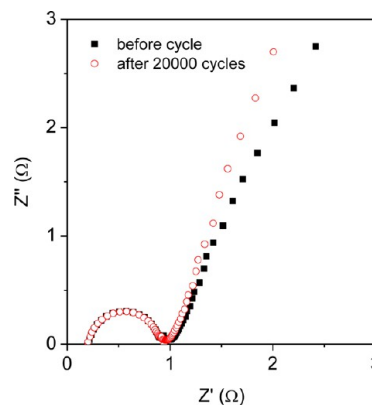

Figure 9. Electrochemical impedance spectra of LTO@GS‖AC hybrid BatCap before and after 20 000 cycles.

in LTO@GS production, which delivers 174.4 mAh g^{-1} at 1 C and maintained 51.9% capacity (vs 1 C) at a high charge/discharge rate of 40 C. With LTO@GS (1.93%) as an anodic electrode, the LTO@GS‖AC BatCap delivers a specific energy of 29.2 Wh kg^{-1} at a specific power of 58.4 W kg^{-1}. When the power output reaches 1782.7 W kg^{-1}, the specific energy retains 13.4 Wh kg^{-1}. A cycle performance test on the BatCap shows that the capacity can hold 90% of its initial value after 20 000 deep cycles at a high charge/discharge rate of 80 C. It is believed that the LTO@GS material synthesized by the one-pot spray-drying assisted solid-phase reaction method can be a promising candidate anode material for the BatCap system.

■ ASSOCIATED CONTENT

Ⓢ Supporting Information

FE-SEM photos of spray-dried precursors; XRD patterns of products calcined at 700 °C for 3 h in Ar/H$_2$ (5%); high-resolution XPS spectra of Ti 2p in LTO@GS composites; Raman spectra of LTO@GS composites; BJH pore size distribution plots and nitrogen adsorption−desorption isotherms of LTO@GS composites; charge/discharge profiles at different rates of LTO@GS electrodes; EIS and equivalent circuit of LTO@GS electrodes; real and imaginary parts of the complex impedance vs $\omega^{-1/2}$ of LTO@GS electrodes; impedance parameters and values of A, dE/dx, and Li$^+$ diffusion coefficient D of LTO@GS electrodes; and rate discharge behaviors of the LTO@GS‖AC BatCap. This material is available free of charge via the Internet at http://pubs.acs.org.

■ AUTHOR INFORMATION

Corresponding Author

*Tel.: +86-21-54744533. Fax: +86-21-54747717. E-mail: ys-he@sjtu.edu.cn.

Notes

The authors declare no competing financial interest.

■ ACKNOWLEDGMENTS

■ REFERENCES

(1) Burke, A. F. Batteries and ultracapacitors for electric, hybrid, and fuel cell vehicles. *Proc. IEEE* **2007**, *95*, 806−820.

(2) Dunn, B.; Kamath, H.; Tarascon, J. M. Electrical energy storage for the grid: a battery of choices. *Science* **2011**, *334*, 928−935.

(3) Conway, B. E. Transition from "supercapacitor" to "battery" behavior in electrochemical energy etorage. *J. Electrochem. Soc.* **1991**, *138*, 1539−1548.

(4) Thackeray, M. M.; Wolverton, C.; Isaacs, E. D. Electrical energy storage for transportation—approaching the limits of, and going beyond, lithium-ion batteries. *Energy Environ. Sci.* **2012**, *5*, 7854−7863.

(5) Conway, B. E. *Electrochemical Supercapacitors: Scientific Fundamentals and Technological Applications*; Springer: Berlin, 1999.

(6) Pasquier, A. D.; Plitz, I.; Menocal, S.; Amatucci, G. A comparative study of Li-ion battery, supercapacitor and nonaqueous asymmetric hybrid devices for automotive applications. *J. Power Sources* **2003**, *115*, 171−178.

(7) Amatucci, G. G.; Badway, F.; Pasquier, A. D. Novel asymmetric hybrid cells and the use of pseudo-reference electrodes in three electrode cell characterization. *Intercalation Compounds for Battery Materials: Proceedings of the International Symposium*; The Electrochemical Society, Inc.: Pennington, NJ, 2000; Vol. *99−24*, pp 344−359.

(8) Amatucci, G. G.; Badway, F.; Pasquier, A. D.; Zheng, T. An asymmetric hybrid nonaqueous energy storage cell. *J. Electrochem. Soc.* **2001**, *148*, A930−A939.

(9) Leng, K.; Zhang, F.; Zhang, L.; Zhang, T. F.; Wu, Y. P.; Lu, Y. H.; Huang, Y.; Chen, Y. S. Graphene-based Li-ion hybrid supercapacitors with ultrahigh performance. *Nano Res.* **2013**, *6*, 581−592.

(10) Wang, Q.; Wen, Z. H.; Li, J. H. A hybrid supercapacitor fabricated with a carbon nanotube cathode and a TiO_2-B nanowire anode. *Adv. Funct. Mater.* **2006**, *16*, 2141−2146.

(11) Cai, Y.; Zhao, B.; Wang, J.; Shao, Z. P. Non-aqueous hybrid supercapacitors fabricated with mesoporous TiO_2 microspheres and activated carbon electrodes with superior performance. *J. Power Sources* **2014**, *253*, 80−89.

(12) Ding, R.; Qi, L.; Wang, H. Porous $NiCo_2O_4$ as an anode material for 4.5 V hybrid Li-ion capacitors. *RSC Adv.* **2013**, *3*, 12581−12584.

(13) Aravindan, V.; Chuiling, W.; Reddy, M. V.; Rao, G. V.; Chowdari, B. V.; Madhavi, S. Carbon coated nano-$LiTi_2(PO_4)_3$ electrodes for non-aqueous hybrid supercapacitors. *Phys. Chem. Chem. Phys.* **2012**, *14*, 5808−5814.

(14) Aravindan, V.; Reddy, M. V.; Madhavi, S.; Mhaisalkar, S. G.; Subba Rao, G. V.; Chowdari, B. V. R. Hybrid supercapacitor with nano-TiP_2O_7 as intercalation electrode. *J. Power Sources* **2011**, *196*, 8850−8854.

(15) Aravindan, V.; Chuiling, W.; Madhavi, S. High power lithium-ion hybrid electrochemical capacitors using spinel $LiCrTiO_4$ as insertion electrode. *J. Mater. Chem.* **2012**, *22*, 16026−16031.

(16) Khomenko, V.; Raymundo-Piñero, E.; Béguin, F. High-energy density graphite/AC capacitor in organic electrolyte. *J. Power Sources* **2008**, *177*, 643−651.

(17) Ohzuku, T.; Ueda, A.; Yamamoto, N. Zero-strain insertion material of $Li[Li_{1/3}Ti_{5/3}]O_4$ for rechargeable lithium cells. *J. Electrochem. Soc.* **1995**, *142*, 1431−1435.

(18) Cheng, L.; Liu, H. J.; Zhang, J. J.; Xiong, H. M.; Xia, Y. Y. Nanosized $Li_4Ti_5O_{12}$ prepared by molten salt method as an electrode material for hybrid electrochemical supercapacitors. *J. Electrochem. Soc.* **2006**, *153*, A1472−A1477.

(19) Bai, Y. J.; Gong, C.; Qi, Y. X.; Lun, N.; Feng, J. Excellent long-term cycling stability of La-doped $Li_4Ti_5O_{12}$ anode material at high current rates. *J. Mater. Chem.* **2012**, *22*, 19054−19060.

(20) Yuan, T.; Wang, K.; Cai, R.; Ran, R.; Shao, Z. P. Cellulose-assisted combustion synthesis of $Li_4Ti_5O_{12}$ adopting anatase TiO_2 solid as raw material with high electrochemical performance. *J. Alloys Compd.* **2009**, *477*, 665−672.

(21) Yuan, T.; Cai, R.; Wang, K.; Ran, R.; Liu, S. M.; Shao, Z. P. Combustion synthesis of high-performance $Li_4Ti_5O_{12}$ for secondary Li-ion battery. *Ceram. Int.* **2009**, *35*, 1757−1768.

(22) Cai, R.; Yuan, T.; Ran, R.; Liu, X. Q.; Shao, Z. P. Preparation and re-examination of $Li_4Ti_{4.85}Al_{0.15}O_{12}$ as anode material of lithium-ion battery. *Int. J. Energy Res.* **2011**, *35*, 68−77.

(23) Wan, Z. N.; Cai, R.; Jiang, S. M.; Shao, Z. P. Nitrogen- and TiN-modified $Li_4Ti_5O_{12}$: one-step synthesis and electrochemical performance optimization. *J. Mater. Chem.* **2012**, *22*, 17773−17781.

(24) Xiang, H. F.; Tian, B. B.; Lian, P. C.; Li, Z.; Wang, H. H. Sol-gel synthesis and electrochemical performance of $Li_4Ti_5O_{12}$/graphene composite anode for lithium-ion batteries. *J. Alloys Compd.* **2011**, *509*, 7205−7209.

(25) Shen, L. F.; Yuan, C. Z.; Luo, H. J.; Zhang, X. G.; Yang, S. D.; Lu, X. J. In situ synthesis of high-loading $Li_4Ti_5O_{12}$-graphene hybrid nanostructures for high rate lithium ion batteries. *Nanoscale* **2011**, *3*, 572−574.

(26) Rai, A. K.; Gim, J.; Kang, S. W.; Mathew, V.; Anh, L. T.; Kang, J.; Song, J.; Paul, B. J.; Kim, J. Improved electrochemical performance of $Li_4Ti_5O_{12}$ with a variable amount of graphene as a conductive agent for rechargeable lithium-ion batteries by solvothermal method. *Mater. Chem. Phys.* **2012**, *136*, 1044−1051.

(27) Jian, Z. L.; Zhao, L.; Wang, R.; Hu, Y. S.; Li, H.; Chen, W.; Chen, L. Q. The low-temperature (400 degrees C) coating of few-layer graphene on porous $Li_4Ti_5O_{12}$ via $C_{28}H_{16}Br_2$ pyrolysis for lithium-ion batteries. *RSC Adv.* **2012**, *2*, 1751−1754.

(28) Kim, J. W.; Shin, M. S.; Kim, J. K.; Kim, H. S.; Koo, K. K. Evaporation crystallization of RDX by ultrasonic spray. *Ind. Eng. Chem. Res.* **2011**, *50*, 12186−12193.

(29) Chen, F. Q.; Cai, C. C.; Cheng, D. G.; Zhan, X. L. Heat transfer characteristics of alumina membrane coated activated carbon with core−shell structure. *Ind. Eng. Chem. Res.* **2013**, *52*, 3653−3657.

(30) Carne-Sanchez, A.; Imaz, I.; Cano-Sarabia, M.; Maspoch, D. A spray-drying strategy for synthesis of nanoscale metal−organic frameworks and their assembly into hollow superstructures. *Nat. Chem.* **2013**, *5*, 203−211.

(31) Luo, J. Y.; Jang, H. D.; Sun, T.; Xiao, L.; He, Z.; Katsoulidis, A. P.; Kanatzidis, M. G.; Gibson, J. M.; Huang, J. X. Compression and aggregation-resistant particles of crumpled soft sheets. *ACS Nano* **2011**, *5*, 8943−8949.

(32) Luo, J. Y.; Jang, H. D.; Huang, J. X. Effect of sheet morphology on the scalability of graphene-based ultracapacitors. *ACS Nano* **2013**, *7*, 1464−1471.

(33) Ruoff, R. Perspective: A means to an end. *Nature* **2012**, *483*, S42.

(34) Wang, W. N.; Jiang, Y.; Biswas, P. Evaporation-induced crumpling of graphene oxide nanosheets in aerosolized droplets: confinement force relationship. *J. Phys. Chem. Lett.* **2012**, *3*, 3228−3233.

(35) He, Y.-S.; Gao, P. F.; Chen, J.; Yang, X. W.; Liao, X.-Z.; Yang, J.; Ma, Z.-F. A novel bath lily-like graphene sheet-wrapped nano-Si composite as a high performance anode material for Li-ion batteries. *RSC Adv.* **2011**, *1*, 958−960.

(36) Luo, J.; Zhao, X.; Wu, J.; Jang, H. D.; Kung, H. H.; Huang, J. Crumpled graphene-encapsulated Si nanoparticles for lithium ion battery anodes. *J. Phys. Chem. Lett.* **2012**, *3*, 1824−1829.

(37) Mao, S.; Wen, Z. H.; Kim, H.; Lu, G. H.; Hurley, P.; Chen, J. A general approach to one-pot fabrication of crumpled graphene-based nanohybrids for energy applications. *ACS Nano* **2012**, *6*, 7505−7513.

(38) Zhou, G.-W.; Wang, J.; Gao, P.; Yang, X.; He, Y.-S.; Liao, X.-Z.; Yang, J.; Ma, Z.-F. Facile spray drying route for the three-dimensional graphene-encapsulated Fe_2O_3 Nanoparticles for lithium ion battery anodes. *Ind. Eng. Chem. Res.* **2013**, *52*, 1197−1204.

(39) Ma, J.; Wang, J.; He, Y.-S.; Liao, X.-Z.; Chen, J.; Wang, J.-Z.; Yuan, T.; Ma, Z.-F. A solvothermal strategy: one-step in situ synthesis of self-assembled 3D graphene-based composites with enhanced lithium storage capacity. *J. Mater. Chem. A* **2014**, *2*, 9200−9207.

(40) Amatucci, G. G.; Badway, F.; Du Pasquier, A.; Zheng, T. An asymmetric hybrid nonaqueous energy storage cell. *J. Electrochem. Soc.* **2001**, *148*, A930−A939.

(41) Li, D.; Müller, M. B.; Gilje, S.; Kaner, R. B.; Wallace, G. G. Processable aqueous dispersions of graphene nanosheets. *Nat. Nanotechnol.* **2008**, *3*, 101−105.

(42) Moser, J.; Punchihewa, S.; Infelta, P. P.; Gratzel, M. Surface complexation of colloidal semiconductors strongly enhances interfacial electron-transfer rates. *Langmuir* **1991**, *7*, 3012−3018.

(43) Wang, J. Z.; Zhong, C.; Chou, S. L.; Liu, H. K. Flexible free-standing graphene-silicon composite film for lithium-ion batteries. *Electrochem. Commun.* **2010**, *12*, 1467−1470.

(44) Kellerman, D. G.; Gorshkov, V. S.; Shalaeva, E. V.; Tsaryev, B. A.; Vovkotrub, E. G. Structure peculiarities of carbon-coated lithium titanate: Raman spectroscopy and electron microscopic study. *Solid State Sci.* **2012**, *14*, 72−79.

(45) Wang, Y. G.; Liu, H. M.; Wang, K. X.; Eiji, H.; Wang, Y. R.; Zhou, H. S. Synthesis and electrochemical performance of nano-sized $Li_4Ti_5O_{12}$ with double surface modification of Ti(III) and carbon. *J. Mater. Chem.* **2009**, *19*, 6789−6795.

(46) Ferrari, A. C.; Robertson, J. Interpretation of Raman spectra of disordered and amorphous carbon. *Phys. Rev. B* **2000**, *61*, 14095−14107.

(47) Yuan, T.; Cai, R.; Shao, Z. P. Different Effect of the Atmospheres on the Phase Formation and Performance of $Li_4Ti_5O_{12}$ Prepared from Ball-Milling-Assisted Solid-Phase Reaction with Pristine and Carbon-Precoated TiO_2 as Starting Materials. *J. Phys. Chem. C* **2011**, *115*, 4943−4952.

(48) Jung, H. G.; Venugopal, N.; Scrosati, B.; Sun, Y. K. A high energy and power density hybrid supercapacitor based on an advanced carbon-coated $Li_4Ti_5O_{12}$ electrode. *J. Power Sources* **2013**, *221*, 266−271.

(49) Naoi, K.; Ishimoto, S.; Isobe, Y.; Aoyagi, S. High-rate nano-crystalline $Li_4Ti_5O_{12}$ attached on carbon nano-fibers for hybrid supercapacitors. *J. Power Sources* **2010**, *195*, 6250−6254.

(50) Choi, H. S.; Im, J. H.; Kim, T. H.; Park, J. H.; Park, C. R. Advanced energy storage device: a hybrid BatCap system consisting of battery−supercapacitor hybrid electrodes based on $Li_4Ti_5O_{12}$−activatedcarbon hybrid nanotubes. *J. Mater. Chem.* **2012**, *22*, 16986−16993.

(51) Ni, J. F.; Yang, L. X.; Wang, H. B.; Gao, L. J. A high-performance hybrid supercapacitor with $Li_4Ti_5O_{12}$-C nano-composite prepared by in situ and ex situ carbon modification. *J. Solid State Electrochem.* **2012**, *16*, 2791−2796.